SUPPLEMENTARY INFORMATION

Enhanced Thermoelectric Performance of Rough Silicon Nanowires

Allon I. Hochbaum[1]*, Renkun Chen[2]*, Raul Diaz Delgado[1], Wenjie Liang[1], Erik C. Garnett[1], Mark Najarian[3], Arun Majumdar[2,3,4], Peidong Yang[1,3,4]

[1]*Department of Chemistry, University of California, Berkeley, CA 94720*

[2]*Department of Mechanical Engineering, University of California, Berkeley, CA 94720*

[3]*Department of Materials Science and Engineering, University of California, Berkeley, CA 94720*

[4]*Materials Sciences Division, Lawrence Berkeley National Laboratory, Berkeley, CA 94720*

**These authors contributed equally to this work*

Supplementary methods and discussion

Thermal bonding of nanowires

Excess thermal anchor deposition by FIB bonding is in the form of a Pt-C composite, is due to low intensity secondary electron emission away from the irradiated region, and is unavoidable. Fig. S1a shows a TEM of such deposition on two bridging Si nanowires near the midpoint between both membranes. The Pt is deposited in the form of

nanoparticles embedded in an amorphous C matrix – a product of the organic ligand decomposition. The nanoparticles do not form a continuous film, and the contribution of the Pt-C composite to thermal conductance is negligible, as demonstrated by repeated bonding and excess deposition on the same nanowire after a first measurement (Fig. S1b). The temperature-dependent thermal conductivity from both measurements is the same.

Calibration of nanowire measurements

To demonstrate the accuracy of these thermal transport experiments, the *k* of SiO_2 nanowires was measured with this apparatus. SiO_2 nanowires were prepared by dry oxidation of VLS-grown Si nanowires at 1000°C for 24 hours. TEM analysis of the oxidized wires showed no crystalline material remaining and energy dispersive X-ray spectroscopy confirmed the presence of abundant O within the nanowires. The *k* of these wires (Fig. S1c) is very close to that of bulk amorphous SiO_2, which was expected since the mean free path of phonons approaches that of the inter-atomic spacing in an amorphous solid. Consequently, no increased boundary scattering was observed as compared to bulk. The experimental error shown in the main text plots of *k* was derived from these measurements using the average error around room temperature (~ 8% at 290K, decreasing with temperature). This error is most likely associated with uncertainty in nanowire diameter determination from SEM and temperature fluctuations during *k* measurement.

Thermal contact resistance

The thermal contact resistance of the Pt-C pads was tested by bonding a 135 nm EE Si nanowire twice, measuring the thermal conductivity after each bonding (Fig. S2a). The second bonding step doubled the contact area of the nanowire and the Pt-C composite, as well as that of the Pt-C composite and the suspended membrane. The measured thermal conductivity of the nanowire was the same before and after the second Pt-C bonding, indicating that the thermal contact resistance of the nanowire-bond-membrane interfaces is negligible (Fig. S2b). Since this nanowire has a higher thermal conductance than the rest of the nanowires used in this study, the ratio of contact resistance to the nanowire resistance is smaller and should be negligible in all the other measurements.

Single nanowire Seebeck coefficient measurement

Due to the difficulty of measuring the local temperature at the closest points of nanowire/metal contacts, the temperature difference along the nanowire was calculated based on a two dimensional heat conduction model to obtain $d\Delta T/dP$. The validity of the model was confirmed by the good agreement between the temperature measured by the two inner Pt electrodes (i.e., average temperature underneath the electrodes) and the simulated average temperature at the same regions. The Seebeck coefficient was determined using $S = \frac{d\Delta V_S}{d\Delta T} = \frac{d\Delta V_S}{dP} \Big/ \frac{d\Delta T}{dP}$. The measured Seebeck coefficient (Fig. 3b, main text) agrees well with literature data[S1-S4], indicating that the electrical properties of the nanowires are largely unaffected at this size scale.

In addition to the 48 nm nanowire discussed in the main text, S and ρ of a smaller diameter (36 nm) nanowire from the same batch were measured. The product of the

power factor and temperature for both wires, as well as near optimally-doped bulk Si (data from Ref. S4) is shown in Fig. S4. The properties of both wires have a similar temperature dependence, though the power factor of the 36 nm nanowire is higher across the entire temperature range measured. The power factor of the nanowires relative to similarly-doped bulk Si decreases with temperature, possibly due to a greater resistivity resulting from increased boundary scattering of electrons. ρ is 1.8 mΩ·cm for the 36 nm nanowire, meaning it may be closer to optimal doping levels than the 48 nm nanowire. Furthermore, if the *k* data for the 52 nm nanowire is used as an upper limit of *k* for the 36 nm nanowire, then ZT reaches at least 0.75 at 300K. Therefore, it is likely that higher thermoelectric efficiencies may be achieved by optimizing the post-growth doping procedure.

The uncertainty of the measured ρ primarily comes from the determination of nanowire diameter by SEM, which has a typical resolution of 1-2 nm based on multiple measurements on different sections of the same nanowire. This translates into a ~ 8% uncertainty in ρ.

The uncertainty of the measured *S* can be estimated as:

$$\frac{\delta(S)}{S} = \delta(\frac{d\Delta V_S}{dP}) \Big/ \frac{d\Delta V_S}{dP} + \delta(\frac{d\Delta T}{dP}) \Big/ \frac{d\Delta T}{dP}$$

where $\delta(x)$ is the uncertainty in *x*. $\frac{d\Delta V_S}{dP}$ normally has less than 1% variation, as the ΔV_S v.s. *P* curves are consistently linear across multiple measurements on the same samples. Since $\frac{d\Delta T}{dP}$ was calculated from the heat conduction model, the uncertainty

origins from the discrepancy between the model and the measurement, which was less than 5% by comparing the modeled and measured average temperature of the two inner Pt electrodes. Therefore, the uncertainty of the measured *S* values would be less than 6%.

Supplementary information references

S1. Geballe, T. H. & Hull, G. W. Seebeck effect in silicon. *Phys. Rev.* **98**, 940 (1955).

S2. Brinson, M. E. & Dunstan, W. Thermal conductivity and thermoelectric power of heavily doped n-type silicon. *J. Phys. C* **3**, 483-491 (1970).

S3. van Herwaarden, A. W. The Seebeck effect in silicon ICs. *Sensors and Actuators*, **6**, 245-254 (1984).

S4. Weber, L. & Gmelin, E. Transport properties of silicon. *Appl. Phys. A* **53**, 136-140 (1991).

Supplementary information figures and legends

Fig. S1

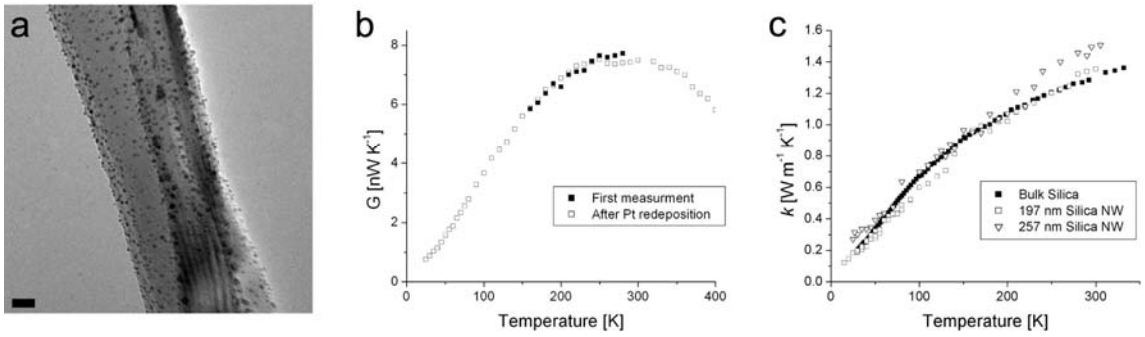

Fig. S1. Nanowire thermal bonding and control experiments. a, TEM image of Pt-C excess deposition on the nanowire away from the irradiated region. The deposition adds thickness to the diameter of the wire as seen in the SEM, so all calculations were based on the diameter determined before Pt bonding. Scale bar is 10 nm. **b,** Thermal conductance of an EE Si nanowire after first bonding with Pt in the FIB (solid squares). The sample broke near one of the pads and was re-bonded at the ends with significant Pt-C deposition over the gap. The conductance measurement after this second bonding (open squares) coincides with the first measurement. Hence, the Pt deposition at the wire ends is a good thermal anchor, but does not contribute significantly to thermal conduction along the wire. **c,** The k of 197 and 257 nm SiO_2 nanowires (open squares and open triangles, respectively) compare quantitatively to that of bulk SiO_2 (solid squares).

Fig. S2

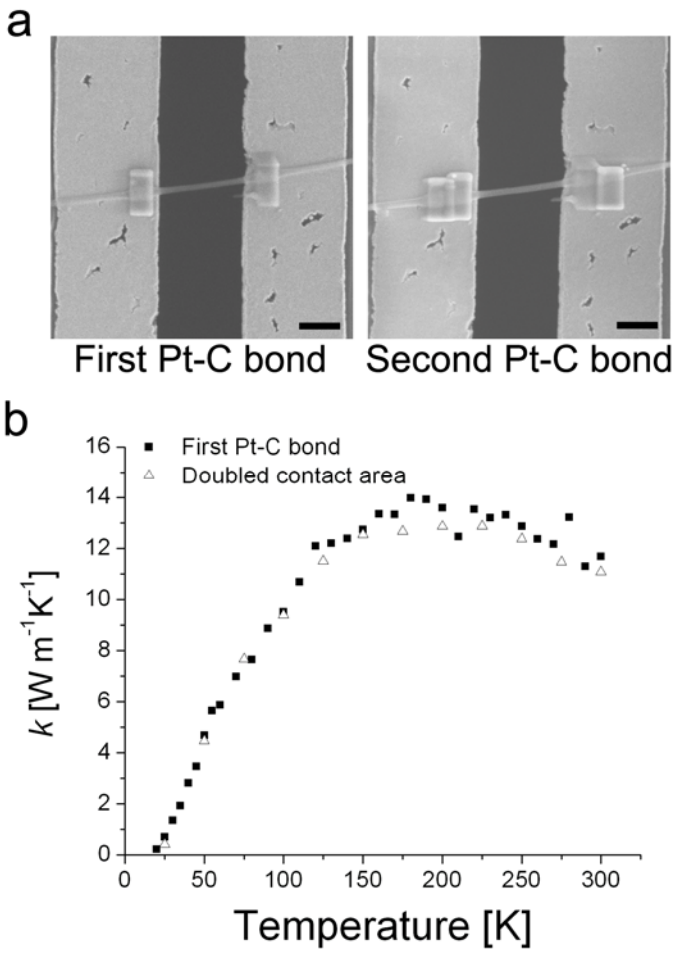

Fig. S2. Thermal contact resistance characterization. a, SEM images of the after both bonding steps. **b,** The measured thermal conductivity of the nanowire before and after doubling the contact area with the suspended membrane. Scale bars are 1 μm.

Fig. S3

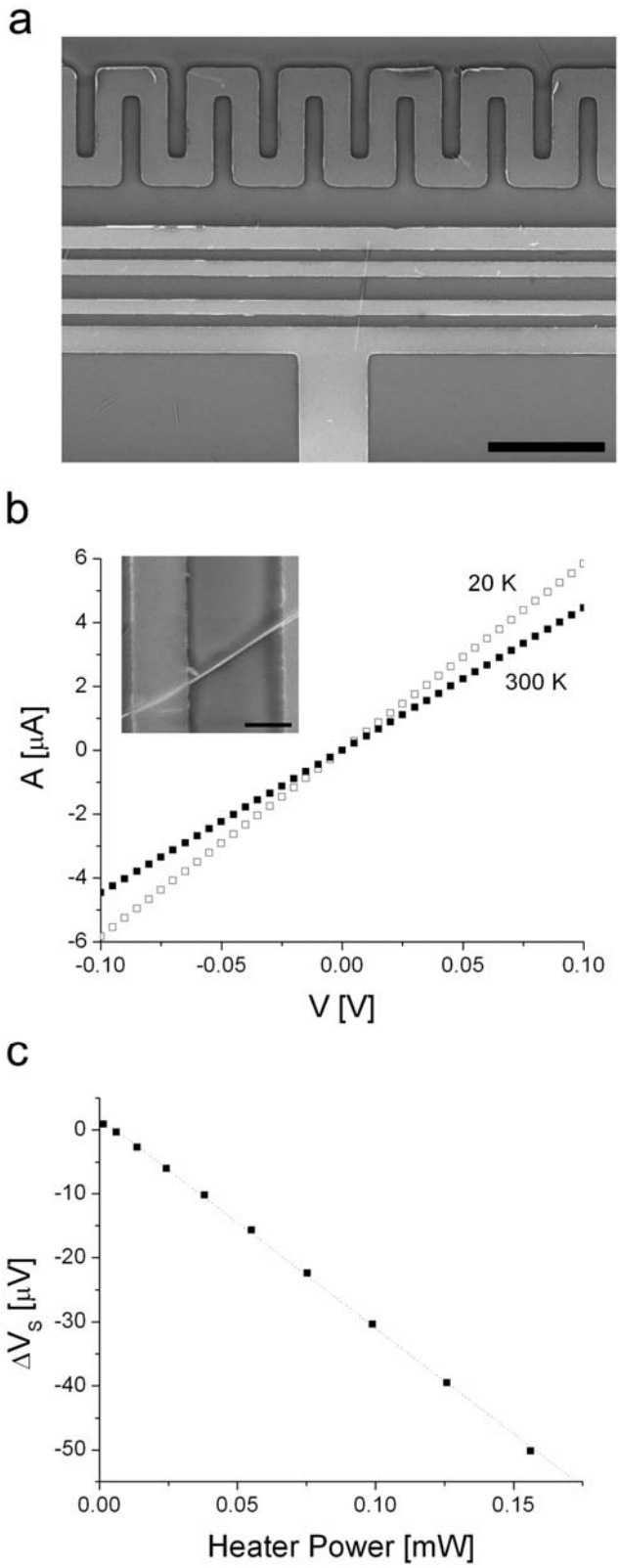

Fig. S3. Single nanowire resistivity and Seeebeck coefficient. a, A SEM image of a typical device used in the present work for electrical ρ and S measurements. The top Pt coil is the heater for S measurement. The inner two Pt electrodes make electrical contacts for the bridging nanowire for (two-probe) ρ and S measurements, and, with the two outer electrodes for four-probe ρ measurements of the nanowire. The scale bar is 10 μm. **b,** I-V behavior of the EE Si nanowire at 300K and 20K. The inset shows an SEM image of the measured device. Scale bar is 300 nm. **c,** The measured Seebeck voltage as a function of power applied to the heater. The relationship is consistently linear across different samples and measurements.

Fig. S4

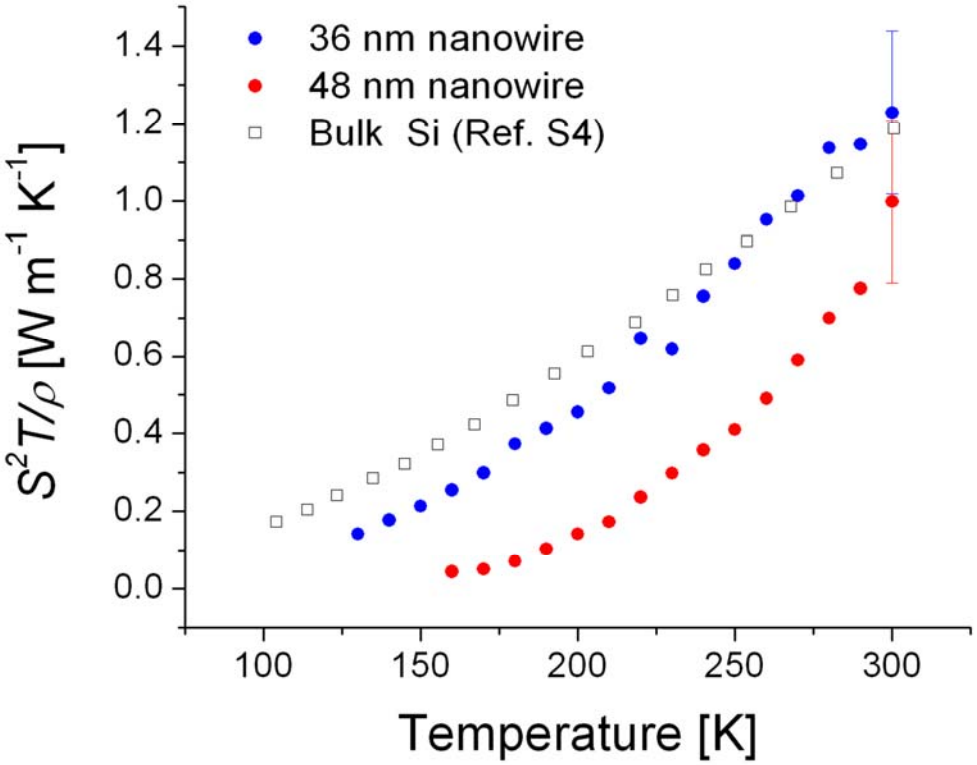

Fig. S4. Temperature dependence of thermoelectric properties of small diameter EE Si nanowires and bulk Si. The product of power factor and temperature for the 36 and 48 nm nanowires (blue and red solid circles, respectively). Bulk Si data (open squares) is taken from Ref. S4 and corresponds to 1.7×10^{19} cm^{-3} As doping, near the predicted optimal doping level.